RSC Advances

ROYAL SOCIETY OF CHEMISTRY

www.rsc.org/advances

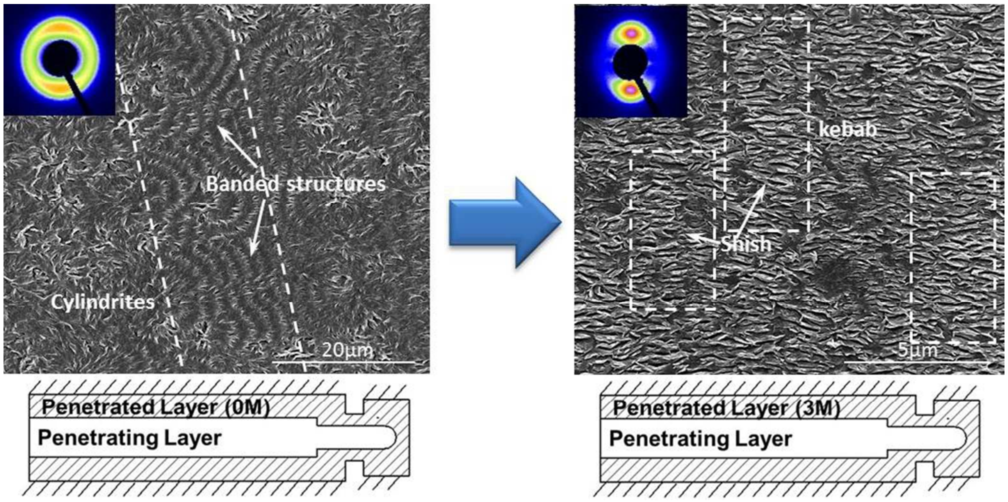

178x88mm (150 x 150 DPI)

An Unusual Transition from Point-like to Fibrillar Crystals in Injection-Molded Polyethylene Articles Induced by Lightly Cross-linking and Melt Penetration

Rui-Yan Zhang, Wei Yang, Kai Zhang, Jian Feng, Chun-Xia Zhu, Xiao-Chao Xia, Shan He, Jian-Ming Feng, Zheng-Ying Liu, Ming-Bo Yang*

Abstract:

Recently, a melt penetrating process in which a first polymer melt is rapidly penetrated by a second polymer melt has been realized on our home-made multi-melt multi-injection molding (MMMIM) machine. Although a great deformation can be provided by the rapid melt penetration process, it has been found that hardly any oriented crystalline structures can be kept and formed due to the quick chain relaxation at high temperatures. In the present work, lightly cross-linked structures were introduced to prolong the relaxation time of linear high density polyethylene (HDPE) molecular chains. The hierarchical structures of MMMIM samples were characterized by scanning electron microscopy (SEM), polarized light microscopy (PLM) and two-dimensional small angle x-ray scattering (2D-SAXS). It was found that the melt penetrating process promoted the formation of cylindritic crystalline structures in the subskin layer, while only isotropic spherulites were formed in subskin layer of corresponding conventional injection molding (CIM) sample. From linear to lightly cross-linked macromolecular chain structure, a transition from cylindritic structures composed of banded-spherulites along the flow direction towards shish-kebabs was observed in the subskin layer of MMMIM samples, and also the distances between two nuclei decreased as well as orientation degree increased gradually in the transition layer. These results indicated that lightly cross-linked HDPE with longer relaxation time are beneficial to keep the point-like nuclei along the flow direction and are helpful for the transition to shish-kebab structures with thread-like nuclei. Modified models are proposed to interpret the mechanism of shish-kebab formation under melt penetrating of samples with lightly cross-linked structures.

Keywords: Melt penetration; Shish-kebab; lightly cross-linked structure

Introduction

The controlling and tailoring of crystalline morphologies are significant for semicrystalline polymers because the physical properties of their products [1-4], are intensively affected by crystalline structures and morphologies. The shish-kebab can markedly increase stiffness and modulus of industrial products, the fibers (from largely lamellar polyethylene) with about 10 GPa modulus, 10 times higher than the unoriented ones, due to the fact that the extended chains (shish) have stronger force in the load direction. In the injected samples, the increase of extended chains (shish) is proposed to cause an increase in the yield stress. It is well known that crystalline morphologies of semi-crystalline polymers are the direct consequence of the thermo-mechanical fields during processing, and spherulites [5], cylindrites [6], shish-kebabs [7] are typical superstructures observed in samples molded by different technologies. However, shish-kebabs are scarcely obtained in conventional injection molding (CIM).

In order to control the crystalline morphologies and meet the requirement of applications, various molding technologies have been invented, including shear-controlled orientation in injection molding (SCORIM) [8], oscillatory shear injection molding (OSIM) [9] and vibration-assisted injection molding (VAIM) [10, 11], etc. The key of these technologies is imposing an intense shear or elongational flow during molding by which polymer chains are stretched along the flow direction, and a transition from a relative isotropic morphology, spherulite, to a highly oriented morphology, shish-kebab, can be observed.

Recently, our group put forward the concept of multi-fluid multi-injection molding (MFMIM) [12, 13], a molding process compared with conventional injection molding (CIM). Gas-assisted injection molding (GAIM), as a typical representive of MFMIM where inertia nitrogen gas acts as the second fluid, has been known to be able to generate interesting crystalline morphologies [14, 15], leading to excellent properties of molded products [16, 17]. Water-assisted injection molding (WAIM), also belonging to MFMIM, is known to show various micro-structures due to the high shear stress and cooling rates with water penetration [18-20].

Among MFMIM technologies, a multi-melt multi-injection molding (MMMIM) process, in which a polymer melt instead of gas or water acts as the second fluid to penetrate the first polymer melt, has been constructed in our laboratory. The key step in MMMIM process is that the mold cavity partially filled with the first polymer melt is penetrated by another high-speed polymer melt, and then the cavity is completely occupied and the sample is cooled down gradually. A schematic representation of MMMIM process is shown in Fig. 1. In this way, a melt penetration process is realized. Compared the melt penetration with other fluids, it is easily figured out that the friction coefficient between two polymer melts is higher than that between polymer melt and gas or water, therefore such a high coefficient will lead to more intensive shear field, which is benefit for the formation of highly oriented crystalline structures such as shish-kebabs [13].

However, the imposing of strong shear flow on semicrystalline polymer melt is insufficient for the formation of shish-kebab structures. Under practical processing conditions, the thermo-mechanical fields during melt-penetrating are complex along the sample thickness [21]. High temperature provided by the second melt may arouse fast relaxation of the oriented molecular chains [22, 23]. Therefore, in order to gain shish-kebab structures, it is helpful to learn about some histories and classic theories of the formation mechanism.

During the past few decades, flow induced crystallization has attracted a lot of interests in many research groups, including Keller [24, 25], Hsiao [23, 26-34], Janeschtz-Kriegl [35-37], Winter [38, 39], Han [40-43] and many others. Base on the experimental results in dilute solutions under flow, de Gennes put forward the coil-stretch transition concept and Keller et al. [24, 25] provided the first evidence of coil-stretch transition in dilute solutions. They thought that only molecules with molecular weight high enough can be oriented at a given shear rate. Hsiao [26] et al. found that only a fraction of molecular chains exhibited coil-stretch transition depending on chain conformation and molecular weight, and the quantity of these molecular chains is as low as the content of shishs. According to the observations of Penning [44] and Chu [45, 46], transient chain conformations instead of the final conformations were given, which proved the prediction of coil-stretch transition by presenting fully stretched chains. In dilute solution crystallization, stretched molecular chains are bound to form shish structures. However, as to the polymer melt, the situation is not as simple as that for dilute solution. Han [40-43] and Hsiao [32] demonstrated that the stretched network is sufficient to induce shish-kebabs without stretching long chains out of the entangled polymer network, only some divergences in which one is important to form network, Han thought the entanglement molecular weight Me was important to form the network while Hsiao argued high molecular weight was significant to form this structure. Certainly, relaxation behavior dependent on temperature is also another important factor. At elevated temperature, macromolecular entanglements in polymer melt are easier to move leading to disentanglement, therefore, the stretched molecular network may not be well retained after shear flow at higher temperature, and they are less effective to induce shish-kebab structure. In Hsiao's study [22] on the lifetime of long-chain precursors, alignments of molecular chains relax quickly at high temperature. Han thought that the degree of orientation and the extent of alignment obviously depend on the relaxation time of critical entanglement molecular weight and other factors at a given temperature and shear field. So the relaxation time of oriented molecular chains must be prolonged in order to gain shish-kebab structures.

In order to suppress the relaxation behaviors, lightly cross-linked structures of HDPE were introduced by light electron-beam irradiation technology. (Even if these cross-linked structures with hardly any gel content, they still provided some 'permanent' entanglement points. When the temperature is above the melting point, these entanglement points cannot disentangle compared with physical entanglement points among linear macromolecular chains.) Many investigations have reported that light electron-beam irradiation technology can change the macromolecular structures, resulting in cross-linking and main-chain scission [47-50]. In this case, the molecular entanglements in bulk melt and the introduced permanent entanglement structures can be stretched and oriented under strong flow provided by the melt penetration process. In addition, the introduced permanent molecular entanglement points cannot slip and disentangle during and after melt penetration compared to the 'physical' transient intermolecular chain entanglement, and hence the relaxation time can be effectively prolonged. In this work, lightly cross-linked HDPE with permanent entanglement points were introduced by different doses of irradiation (see supporting material), and the samples were imposed on the melt penetration in order to experience strong shear flow, and we focused on the combined influence of melt-penetration and lightly cross-linked structures on the crystalline morphologies of samples which were characterized by polarized light microscopy (PLM), scanning electron microscopy (SEM), two-dimensional small angle x-ray scattering (2D-SAXS).

Experiment

Material

High-density polyethylene resin (HDPE, Model: 2911) was obtained from Fushun Petroleum Chemical Co. Ltd, P.R. China, whose melt flow rate (MFR) is 20 g/10 min (190°C/2.16kg, ASTM D1238). The weight-average molecular weight (Mw) is 1.42×10^5 g/mol and the polydispersity is 3.3.

Sample Preparation

The light electron-beam irradiation was carried out at room temperature by using SINR electron accelerator in Shanghai Institute of Applied Physics, with energy of 3.0 MeV. The electron beam current density is 6.54 mA. The irradiation doses are 2 Mrad and 3 Mrad, respectively. The basic characteristics of electron-irradiated PE (including gel permeation chromatography, rheology behaviors and topological structures) were given in Supporting Information. The rheological, GPC and DSC results of 0Mrad, 2Mrad and 3Mrad indicated that the relaxation time was prolonged remarkably from 0.005s to 4s without any change in molecular weight. From rheology and successive self-nucleation annealing (SSA) results, the networks of lightly cross-linked structures in 3Mrad sample are more stable than those in 2Mrad. In fact, the gel content is too small to be detected in all samples. But it is known that light electron beam can make HDPE cross-linked [47-50]. So we still use the conception of lightly cross-linked structures instead of branching structures in this work.

The melt penetration process is performed on our MMMIM instrument. A schematic diagram of the MMMIM instrument used is shown in Fig.2. It consists of two injection units, an SM60HC injection molding machine by which the first polymer is plasticized and injected into the cavity to form the penetrated layer of the final sample and an SHJ20 micro-pneumatic injection molding machine (the injection pressure, air pressure, is supplied by an air compressor) by which the penetrating material is plasticized and injected to penetrate the first polymer melt. The two injection units are controlled independently so that the delay time between the onsets of the two units can be adjusted. The samples experienced melt penetration process with the same irradiation dose of n Mrad are marked as ‘nM’ and the samples experienced no melt penetration process with irradiation dose of n Mrad are marked as ‘nC’, as shown in Table 1. The processing parameters of MMMIM and CIM processes are listed in Table 2.

Table 1 Names of samples molded by different processing with various doses of irradiation.

Processing Dose of irradiation	Melt penetration	Non-melt-penetration
Without any irradiation	0M	0C
2 Mrad	2M	2C
3 Mrad	3M	3C

Table 2 Processing parameters for both melt-penetration (MMMIM) and non-melt-penetration (CIM) process.

Parameters	Non-melt-penetration	Melt-penetration	
		Injection Unit 1	Injection Unit 2
Injection pressure (Mpa)	48	48	48
Melt temperature (◦C)	220	220	220
Mold temperature (◦C)	100	100	100
Delay time (s)	~	15	
Cool time (s)	150	150	
Injection volume (%)	~	50	50

The specimens for scanning electron microscope (SEM) and polarized light microscopy (PLM) observations were cut in the direction parallel to flow direction (FD), as illustrated in Fig.3. First, the MMMIM molded sample with a thickness of 5mm was cut at the position 30 mm away from the gate of MMMIM parts; then the slices (20 μm for PLM and 50 μm for SEM observation) were cut by microtome from the central part of the sample along the flow direction. The length along the FD is about 5mm and the length along the ND is 5mm. The samples for 2D-SAXS measurement were cut from the 70 mm wide and 5 mm thick specimen into a 20mm×1 mm (width-thickness) piece, and the samples were obtained from 30 mm far away from the gate. The X-ray beam with 0.4 mm width was normal to the FD-ND plane, moving from exterior to inner.

Morphological observations

As shown in Fig. 3, the obtained slices were sandwiched by penetrated layer, about 50 μm thickness. The slices were etched by mixture of mixed acid and permanganic potassium for 3.5h. After the surfaces were fully washed, dried and coated with a thinner layer of gold, the crystalline morphologies were observed by SEM instrument, FEI (INSPECT-F), at an accelerating voltage of 20 kV. The slices with the thickness of 20 μm were observed by Olympus BX-51 polarized light microscopy (PLM) with a Micropublisher RTV 5.0 digital camera (DC).

Two-dimensional small-angle X-ray scattering (2D-SAXS)

Two-dimensional small-angle X-ray scattering (2D-SAXS) were performed at the beamline BL16B1 of Shanghai Synchrotron Radiation Facility (SSRF, shanghai, China). For 2D-SAXS characterization, the wavelength of X-ray is 0.124 nm and beam size is 0.4×1.0 mm. The 2D-SAXS patterns are collected by an X-ray CCD detector (Model Mar165, 2048×2048 pixels of 80.56×80.56 μm). The distance of sample-to-detector is 2000 mm. One dimensional scattering intensity distributions have been integrated from the two-dimensional scattering patterns in particular region. For the isotropic samples a 360° integration of intensity at each scattering vector q (q=4π(sinθ)/λ, where 2θ is the scattering angle and λ is the wavelength) has been calculated. The SAXS data were subtracted from background scattering before calculating the orientation function.

The degree of crystal orientation at different regions could be calculated by Hermans’ orientation function f described as follows:

$$f = \frac{3(\cos^2\phi) - 1}{2} \qquad (1)$$

where $(\cos^2\phi)$ was defined as:

$$(\cos^2\phi) = \frac{\int_0^{\frac{\pi}{2}} I(\phi)\sin\phi(\cos^2\phi)d\phi}{\int_0^{\frac{\pi}{2}} I(\phi)\sin\phi d\phi} \qquad (2)$$

where φ is the angle between flow direction and the normal vector of a given (hk0) lattice plane and I(φ) is the intensity diffracted from (hk0) planes normal to the crystallographic direction. The limit values of orientation factor f taking φ=0 as the flow direction, are -0.5 for a perfectly normal to the flow direction and 1.0 for a perfectly parallel orientation. When f=0, there is random orientation in the sample.

Results and Discussion

Crystalline morphologies

The crystalline morphologies of subskin layers in the samples without experiencing melt penetration process molded by conventional injection molding (CIM) were shown in Fig. 4. All the common spherulites composed of randomly distributed lamella looks like ‘snowballs’, whose diameters are as large as about 3-5 µm. The main crystalline features in the other layers are also common spherulites, which are omitted here. The absence of the oriented structures is resulted from the high mold temperature (100 ◦C) used in this work which leads to a fast relaxation of oriented structures at the solidification stage, therefore, the crystalline morphologies in the subskin layer are distinct from the general fact that a thin layer of highly oriented structure exists in CIM part due to the quick solidification close to the mold wall [51]. There is no difference in the crystalline morphology of all non-melt penetration samples with various irradiation doses, which demonstrates that the lightly cross-linked PE cannot be adjusted to induce the formation of shish-kebabs without experiencing a large strain provided by melt penetration process.

Fig. 5 shows the PLM and SEM micrographs of 0M sample (without irradiation treatment). From PLM results, a large number of cylindritic structures were formed both in penetrated and penetrating layer, displaying an attractive double skin-core structure. From the SEM micrographs with higher magnification, it was clearly seen that the cylindritic structures of 0M part were composed of many banded spherulites aligned tightly along the flow direction, and compact and imperfect cylindrites were formed in the subskin layer while looser and perfect cylindritic structures appeared at the transition layer, which was reported by our group previously [12]. The banded-spherulites distributed disorderly in both skin and core layers but with different diameters, whose diameters are as large as 10 µm in skin layer and 300 µm in core region. In our previous work [14], it was concluded that the banded spherulites could be induced by certain flow field. The flow intensity is less than the upper critical value, exceeding the value will lead to the formation of oriented lamella, and at the same time, is greater than the lower critical value required for the onset of eligible lamellar twisting. Owing to the intense flow induced by melt penetrating, polymer melt was subjected to flow with shear stress exceeding the lower critical value, so banded spherulites and cylindrites were formed in the melt penetrating samples. In addition, the sizes of banded spherulites in skin layer are smaller than those in core layer, which is due to the faster cooling rate in skin layer close to mold wall.

Fig. 6 shows the PLM and SEM micrographs of 2M sample with an irradiation dose of 2 Mrad. A large number of cylindrites were observed among all layers except for the skin layer at the first glance, as shown in the PLM observation. From SEM micrographs, it is interesting that common spherulites rather than banded spherulites were formed in the skin layer, whose diameter is as large as 3-5 µm, see Fig. 6(a). Since the diameters of crystals in 2M are much smaller than those (10 µm) of 0M, the lamella can only be twisted under greater stress condition in order to balance the surface stress [52-55]. The cylindrites composed of banded structures with various diameters and compactness degree were observed in other layers of 2M part, as shown in Fig. 6(b)-(d). One can see that the diameters of cylindrites increased from 10 µm in subskin layer to 50 µm in transition layer, and to 200 µm in the core layer finally, which were resulted from the various cooling rates from the mold wall to the center. The cooling rate in the center is much slower than that close to mold wall, therefore, the diameters of cylindrites in core layer is larger than those in skin layer. The cylindrites composed of banded structures were formed in core layer due to the prolongation of relaxation time of macromolecular chains in 2M system, and when these network structures were subjected to shear or elongational flow, the molecular networks were stretched and became ordered aligned. These privileged alignments acted as the nuclei arranged along the flow direction [36], and the row nuclei were retained for the prolongation of relaxation time in 2M part, leading to the formation of cylindrites in core layer, as shown in Fig. 6(d). For comparison, only disorded banded spherulites were formed in core layer of 0M because the relaxation time was too short to reserve the row nuclei, see Fig. 5(d).

An even prolonged relaxation time was gained in 3M sample with increased dose of irradiation. To our surprise, shish-kebab structures rather than cylindrites were observed in the subskin layer, where crystalline morphologies were in good accordance with the penning’s observation in 1960s [63]. In Janschitz-Kriegl’s study, a crystalline morphological transition from number of point-like nuclei towards threadlike nuclei crystalline structures was achieved by increasing the intensity of shear [64]. The transition from saturation of point-like nuclei to oriented structures was also observed with increasing shear rate or time. Although the crystalline structures grown from the point-like nuclei in these previous literatures were common spherulites rather than cylindrites observed in this work, we found no fibrillar crystals or bundle structures formed in our observation and only point-like domains closely along the flow direction impinged against each other. The shishes are arranged along the flow direction from which the oriented lamella (kebabs) epitaxially grew [32], such structures were also observed by some newly developed molding technologies with special stress field while were seldom observed in CIM [57].

From the transition layer of 3M sample, one can see cylindrites with tightly arranged banded structures compared with cylindrites in the same layer of other samples, see Fig. 7(c). The banded structures were restricted by each other along the flow direction, thus they grew perpendicular to flow direction with a width of 60μm, looking like twisted kebabs. In the core layer, relatively smaller banded-spherulites rather than bigger banded-spherulites were observed, whose diameters are 30-50 μm, much smaller than those (about 200 μm) in the core layer of sample 0M. The relaxation time was so long that much more ordered alignments can be retained, and these privileged alignments acted as nuclei from which lamella grew, therefore the diameters of banded-spherulites were confined and arranged disorderly in the whole core regime.

In order to clearly and accurately describe the compactness of cylindrites with banded structures, the distances between two nuclei (d) and radius of crystals (r) in transition layer were measured from SEM microphotograph. The distances (d) decreased from about 50 μm in 0M part to only about 10 μm in 3M sample with increasing dose of irradiation, and the average crystals radius (r) was about 30 μm in all samples. The ratio (R) of nuclei distance (d) to crystals diameter (2r) can be used to judge whether the crystalline growth along the flow direction restricted by two nuclei. The ratios (R) of all samples are less one, therefore, the crystalline growth between two nuclei along the flow direction were interacted, which demonstrated the cylindrites were formed. And we can see the ratio decreased from 0.58 in 0M part to only 0.17 in 3M sample with increasing dose of irradiation, illustrating that the compactness increased and more nuclei reserved arranged along the flow direction, as shown in Fig. 8.

Molecular orientation

Fig. 9 shows the selected 2D-SAXS patterns at various locations in 0M, 2M and 3M samples from skin to core layer. At the skin layer of all samples subjected to melt penetration, the scattering patterns show isotropic signal suggesting that isotropic structures were formed, and as observed in the microscopy observations (see Fig. 5-7(a)), common and banded spherulites were formed disorderly in this region. Two meridional maximum and equatorial streak signals first appeared at the subskin layer of 3M part, demonstrating the presence of fibrillar nuclei structures, that is, shishes, along the flow direction and oriented structures perpendicular to the flow direction, also in accordance with SEM observation (see Fig. 7(b)). From the transition layer to core layer, the scattering maxima changed from anisotropic to isotropic signal, which indicated a decline of molecular orientation.

In order to reveal the orientation degree of the molecular chains quantitatively, the scattering intensity distribution along the azimuthal angle between 0 and 180◦ was integrated and the orientation of molecular structures can be visually reflected by the azimuthal width shown in Fig.10 (a)-(c). The orientation degrees in the skin layer of all MMMIM samples are almost 0 due to the fact that they are too low to be calculated, illustrating that no molecular orientation along the flow direction. The orientation factors in 3M part decreased from 0.6 in the subskin layer to 0.24 in the core layer, due to the existence of shish-kebab structures in the subskin layer. Then the orientation factor decreased to core layer gradually owing to random distribution of banded-spherulites, see Fig. 7(d). Meanwhile, the orientation factor increased from 0.32 to 0.52 with decreasing of the distance between two nuclei from 0M to 3M in the transition layer, as shown in Fig. 8. Certainly, the orientation parameter (0.52) of samples with cylindrites with the most compact banded structures is less than that of samples with shish-kebabs (0.6), illustrating that the crystals with thread-like nuclei had higher orientation than those crystals with point-like nuclei even arranged tightly along the flow direction.

Long Period

To describe the evolution of lamellar long period (L), one-dimensional scattering intensity distributions of meridianal direction are plotted in Fig. 11. The peak value q is related to the long period (L) corresponding to the thickness of lamellar and amorphous region between two lamella, which can be calculated by Bragg equation:

$$L = \frac{2\pi}{q_{max}} \tag{3}$$

As shown in Fig. 11, the calculated long periods of all layers in 0M samples are nearly constant, about 23 nm, only slightly smaller than those in 2M samples and about 2 nm smaller than those in 3M specimens. That the long periods of all layers in 0M an 2M are almost invariant may result from that the cylindritic structures observed are still grown from point-like nuclei, and only point-like nuclei of cylindritic structures along the flow direction while those of spherulites are distributed randomly. Therefore, the crystalline structures are the same and show no difference of long periods. Form Fig. 11, the long periods in 3M sample are much larger than those in 0M part. However, long period of the subskin layer is about 1 nm less than that of other layers in 3M sample. And this observation indicated that the higher nucleation density lead to smaller long period [23, 26].

The formation process and mechanism discussion

Although the molecular mechanism of the formation of shish-kebab and cylindritic structures is still in argument, our current result is one good example for demonstrating that lightly cross-linked structures can facilitate the formation of shish-kebab structures. Therefore, combining previous researches and our comprehension of the formation mechanism and model of shish-kebabs and cylindrites, the molecular mechanism of the formation of the crystalline structures observed in this work was discussed here.

The cylindrites composed of banded structures, different from the observations in literatures, [40, 41, 43, 58-62] were formed without fibrillar crystals or the bundle structures acting as the nucleation sites from which crystals grew, and they looked like the repeat banded structures impinging against each other closely along the flow direction. According to the results here and our previous work [12], the process of cylindritic structures were formed as below.

The molecular chains in the blank melt are random coils initially; then the melt is subjected to shear and elongational flow due to melt penetrating, and the molecular network can be stretched and compacted along the flow direction [63], which lead to high-density local alignments similar to the process of density fluctuations during the induction stage of crystallization [64, 65]. These precursors with compact local alignments were along the flow direction, which may be the quasi-ordered clusters whose size dependent on the intensity of the flow [66], or metastable, noncrystalline phase [67], or smectic domains [68, 69]. The faster cooling rate close to mold wall made the physical entanglement strong enough to be reserved and act as the point-like row nuclei, and the surrounding molecular chains were absorbed by these nuclei and formed crystals radially. The crystal growth can only take place normal to the flow direction in the compacted region, leading to the formation of cylindrites as shown in Fig. 12 I(b). However, during cooling process, the center of the sample where the cooling rate was much slower, the physical entangling points were unstable due to the fact that they were in dynamic balance and changed their positions easily and rebuilt somewhere else [70]. In other words, the oriented precursors relaxed sufficiently before crystallization due to the weak physical network at high temperature. So banded-spherulites were formed randomly rather than cylindrites along the flow direction, as shown in Fig. 12 I(a).

When some permanent entanglement points are introduced in lightly cross-linked samples, the chemical entanglements are much more stable than physical entanglements at high temperature, and they will cause more physical entangling points at the same time. Therefore, the relaxation time of molecular chains in 2M part instantly increased. (see supporting material). When the polymer melt were sheared or elongated during melt penetrating process, the row precursors along the flow direction appeared with the restriction of physical and permanent entangling points. The precursors behaved as the row nuclei for the epitaxial growth of banded structures and can be retained easily, as shown in Fig. 12 II, leading to the formation of cylindrites observed in 2M part (see Fig. 6).

When more stable permanent entangle points in lightly cross-linked structures were introduced, the relaxation time in sample 3M increased greatly compared with that in 0M system with only physical networks (see supporting material). According to Mykhaylyk [71] and Peters [56], when the longest relaxation time increased, the shear rates above the inverse Rouse time of chains were easier to achieve, and it became easier to orient and stretch the molecular chains, then the molecular alignments formed the fibrillar nuclei or bundle of alignments (shishes) along the flow direction. From 0M to 3M samples, the transition from cylindrites composed of point-like crystals along the flow direction towards shish-kebab structures was observed, which seemed that there was a critical molecular entanglement depending on the temperature and flow subjected in subskin layer of samples. After melt penetration and the stretched alignments started to relax gradually, the physical entanglements and permanent entanglement points provided by lightly cross-linked structures could make the stretched chain segments confined tightly between entangling points, thus the stretched alignments could be kept in their oriented state. Additionally, since the long chains in electron irradiation systems with different doses of irradiation were constant, the increase of relaxation time in 3M system contributed a number of entanglement points instead of long chains. Then the stretched alignments acting as the fibrillar nuclei (shishes) are arranged along the flow direction on which oriented lamella (kebabs) epitaxially grew by absorbing the surrounding random molecular chains. The final result is the formation of shish-kebab structures, as shown in Fig. 12 III.

Conclusion

This is the first time that a transition from point-like crystals along the flow direction (cylindrites) towards thread-like nuclei crystals (shish-kebabs) has been achieved by introducing lightly cross-linked structures, demonstrating that more entanglement points in original melt could promote the formation of shish-kebabs under a certain flow condition induced by melt penetrating process. Only isotropic crystalline morphology spherulites were observed in non-melt penetration process. According to the microscopy observations and 2D-SAXS results, it was concluded that the combination of melt penetration and lightly cross-linked structures can induce fascinating crystalline morphologies, especially the transition from cylindrites to shish-kebab.

Acknowledgement

We would like to express our sincere thanks to the National Natural Science Foundation of China for financial support (21174092, 51473105， 51421061) and the Major State Basic Research Development Program of China (973 program) (Grant No. 2012CB025902). The authors also thank Mr. Chao-liang Zhang for his kind assistance in morphological observations. We are grateful for that the 2D-SAXS experiments can be performed at the beamline BL16B1 of Shanghai Synchrotron Radiation Facility (SSRF, shanghai, China).

Reference

College of Polymer Science & Engineering, and the State Key Laboratory of Polymer Materials Engineering, Sichuan University, Chengdu 610065, P.R. China. Fax: 02885405234; Tel: 02885401988; E-mail: yangmb@scu.edu.cn.

1 B. Schrauwen, L. v. Breemen, A. Spoelstra, L. Govaert, G. Peters and H. Meijer, *Macromolecules*, 2004, **37**, 8618-8633.
2 M. Kristiansen, M. Werner, T. Tervoort, P. Smith, M. Blomenhofer and H.-W. Schmidt, *Macromolecules*, 2003, **36**, 5150-5156.
3 L. Balzano, S. Rastogi and G. W. Peters, *Macromolecules*, 2009, **42**, 2088-2092.
4 Z. Bashir, J. Odell and A. Keller, *Journal of materials science*, 1986, **21**, 3993-4002.
5 R. Pantani, I. Coccorullo, V. Speranza and G. Titomanlio, *Progress in polymer science*, 2005, **30**, 1185-1222.
6 A. Keller, *Journal of Polymer Science*, 1956, **21**, 363-379.

7 H. Fukushima, Y. Ogino, G. Matsuba, K. Nishida and T. Kanaya, *Polymer*, 2005, **46**, 1878-1885.
8 G. Kalay and M. J. Bevis, *Journal of Polymer Science Part B: Polymer Physics*, 1997, **35**, 415-430.
9 L. Xu, C. Chen, G.-J. Zhong, J. Lei, J.-Z. Xu, B. S. Hsiao and Z.-M. Li, *ACS applied materials & interfaces*, 2012, **4**, 1521-1529.
10 A. M. Tom, A. Kikuchi and J. P. Coulter, *Specialized Molding Techniques: Application, Design, Materials and Processing*, 2002, 245.
11 L. Youbing, L. Yongheng, G. Xueqin, Y. Yi, K. Wenti and S. Kaizhi, *Journal of Polymer Science Part B: Polymer Physics*, 2005, **43**, 13-21.
12 K. Zhang, Z. Liu, B. Yang, W. Yang, Y. Lu, L. Wang, N. Sun and M. Yang, *Polymer*, 2011, **52**, 3871-3878.
13 R.-Y. Zhang, W. Yang, J.-J. Wu, J. Feng, J.-M. Feng, B.-H. Xie and M.-B. Yang, *RSC Advances*, 2014, **4**, 31960-31968.
14 L. Huang, W. Yang, B. Yang, M. Yang, G. Zheng and H. An, *Polymer*, 2008, **49**, 4051-4056.
15 G.-Q. Zheng, L. Huang, W. Yang, B. Yang, M.-B. Yang, Q. Li and C.-Y. Shen, *Polymer*, 2007, **48**, 5486-5492.
16 C. Li, J. Shin, A. Isayev and H. Lee, *Polymer Engineering & Science*, 2004, **44**, 992-1002.
17 R. Der Chien, S.-C. Chen and Y.-C. Chen, *Plastics, rubber and composites*, 2002, **31**, 336-343.
18 H.-X. Huang, B. Wang and W.-W. Zhou, *Composites Part B: Engineering*, 2012, **43**, 972-977.
19 S.-J. Liu, M.-J. Lin and Y.-C. Wu, *Composites science and technology*, 2007, **67**, 1415-1424.
20 S. J. Liu, W. R. Lin and K. Y. Lin, *Polymers for Advanced Technologies*, 2011, **22**, 2062-2068.
21 J. C. Viana, A. M. Cunha and N. Billon, *Polymer*, 2002, **43**, 4185-4196.
22 G. Kumaraswamy, J. A. Kornfield, F. Yeh and B. S. Hsiao, *Macromolecules*, 2002, **35**, 1762-1769.
23 L. Yang, R. H. Somani, I. Sics, B. S. Hsiao, R. Kolb, H. Fruitwala and C. Ong, *Macromolecules*, 2004, **37**, 4845-4859.
24 A. Keller and S. Z. Cheng, *Polymer*, 1998, **39**, 4461-4487.
25 M. Miles and A. Keller, *Polymer*, 1980, **21**, 1295-1298.
26 R. H. Somani, B. S. Hsiao, A. Nogales, S. Srinivas, A. H. Tsou, I. Sics, F. J. Balta-Calleja and T. A. Ezquerra, *Macromolecules*, 2000, **33**, 9385-9394.
27 R. H. Somani, B. S. Hsiao, A. Nogales, H. Fruitwala, S. Srinivas and A. H. Tsou, *Macromolecules*, 2001, **34**, 5902-5909.
28 R. H. Somani, L. Yang, B. S. Hsiao, T. Sun, N. V. Pogodina and A. Lustiger, *Macromolecules*, 2005, **38**, 1244-1255.
29 R. H. Somani, L. Yang, B. S. Hsiao, P. K. Agarwal, H. A. Fruitwala and A. H. Tsou, *Macromolecules*, 2002, **35**, 9096-9104.
30 P. K. Agarwal, R. H. Somani, W. Weng, A. Mehta, L. Yang, S. Ran, L. Liu and B. S. Hsiao, *Macromolecules*, 2003, **36**, 5226-5235.
31 R. H. Somani, L. Yang and B. S. Hsiao, *Physica A: Statistical Mechanics and its Applications*, 2002, **304**, 145-157.
32 R. H. Somani, L. Yang, L. Zhu and B. S. Hsiao, *Polymer*, 2005, **46**, 8587-8623.
33 S. Ran, X. Zong, D. Fang, B. S. Hsiao, B. Chu and R. A. Phillips, *Macromolecules*, 2001, **34**, 2569-2578.
34 T. Servay, R. Voelkel, H. Schmiedberger and S. Lehmann, *Polymer*, 2000, **41**, 5247-5256.
35 H. Janeschitz-Kriegl and E. Ratajski, *Colloid and Polymer Science*, 2010, **288**, 1525-1537.
36 H. Janeschitz-Kriegl, *Crystallization modalities in polymer melt processing*, Springer, 2009.
37 H. Janeschitz-Kriegl and E. Ratajski, *Polymer*, 2005, **46**, 3856-3870.
38 N. V. Pogodina, V. P. Lavrenko, S. Srinivas and H. H. Winter, *Polymer*, 2001, **42**, 9031-9043.
39 N. Pogodina, S. Siddiquee, J. Van Egmond and H. Winter, *Macromolecules*, 1999, **32**, 1167-1174.
40 C. Zhang, H. Hu, D. Wang, S. Yan and C. C. Han, *Polymer*, 2005, **46**, 8157-8161.
41 C. Zhang, H. Hu, X. Wang, Y. Yao, X. Dong, D. Wang, Z. Wang and C. C. Han, *Polymer*, 2007, **48**, 1105-1115.
42 L. Zhang, W. Shi, H. Cheng and C. C. Han, *Polymer*, 2014, **55**, 2890-2899.
43 Y. Wang, K. Meng, S. Hong, X. Xie, C. Zhang and C. C. Han, *Polymer*, 2009, **50**, 636-644.
44 A. Pennings and M. Pijpers, *Macromolecules*, 1970, **3**, 261-262.
45 D. E. Smith and S. Chu, *Science*, 1998, **281**, 1335-1340.
46 D. E. Smith, H. P. Babcock and S. Chu, *Science*, 1999, **283**, 1724-1727.
47 A. Charlesby, *Proceedings of the Royal Society of London. Series A. Mathematical and Physical Sciences*, 1952, **215**, 187-214.
48 R. Kitamaru and L. Mandelkern, *Journal of Polymer Science Part B: Polymer Letters*, 1964, **2**, 1019-1023.
49 A. Chawla and L. St Pierre, *Journal of Applied Polymer Science*, 1972, **16**, 1887-1891.
50 A. Keller and G. Ungar, *Radiation Physics and Chemistry (1977)*, 1983, **22**, 155-181.
51 G.-J. Zhong, L. Li, E. Mendes, D. Byelov, Q. Fu and Z.-M. Li, *Macromolecules*, 2006, **39**, 6771-6775.
52 H. Keith and F. Padden Jr, *Polymer*, 1984, **25**, 28-42.
53 M. Kunz, M. Drechsler and M. Möller, *Polymer*, 1995, **36**, 1331-1339.
54 H. Keith, F. Padden Jr, B. Lotz and J. Wittmann, *Macromolecules*, 1989, **22**, 2230-2238.
55 J. Hobbs, A. Humphris and M. Miles, *Macromolecules*, 2001, **34**, 5508-5519.
56 J.-W. Housmans, R. J. Steenbakkers, P. C. Roozemond, G. W. Peters and H. E. Meijer, *Macromolecules*, 2009, **42**, 5728-5740.
57 J. Martínez-Salazar, J. G. Ramos and J. Petermann, *International Journal of Polymeric Materials*, 1993, **21**, 111-121.
58 R.-C. Zhang, Y. Xu, A. Lu, K. Cheng, Y. Huang and Z.-M. Li, *Polymer*, 2008, **49**, 2604-2613.
59 M. Seki, D. W. Thurman, J. P. Oberhauser and J. A. Kornfield, *Macromolecules*, 2002, **35**, 2583-2594.
60 S. Liedauer, G. Eder and H. Janeschitz-Kriegl, *International Polymer Processing*, 1995, **10**, 243-250.
61 S. Liedauer, G. Eder, H. Janeschitz-Kriegl, P. Jerschow, W. Geymayer and E. Ingolic, *International Polymer Processing*, 1993, **8**, 236-244.
62 G. Kumaraswamy, R. Verma, A. Issaian, P. Wang, J. Kornfield, F. Yeh, B. Hsiao and R. Olley, *Polymer*, 2000, **41**, 8931-8940.
63 T. Hashimoto, H. Murase and Y. Ohta, *Macromolecules*, 2010, **43**, 6542-6548.
64 N. J. Terrill, P. A. Fairclough, E. Towns-Andrews, B. U. Komanschek, R. J. Young and A. J. Ryan, *Polymer*, 1998, **39**, 2381-2385.
65 M. Imai, K. Kaji and T. Kanaya, *Physical review letters*, 1993, **71**, 4162.
66 B. Monasse, *Journal of materials science*, 1992, **27**, 6047-6052.
67 R. Androsch, M. L. Di Lorenzo, C. Schick and B. Wunderlich, *Polymer*, 2010, **51**, 4639-4662.
68 L. Li and W. H. de Jeu, *Macromolecules*, 2003, **36**, 4862-4867.
69 L. Li and W. H. de Jeu, *Physical review letters*, 2004, **92**, 075506.
70 F. Zuo, J. K. Keum, L. Yang, R. H. Somani and B. S. Hsiao, *Macromolecules*, 2006, **39**, 2209-2218.
71 O. O. Mykhaylyk, P. Chambon, R. S. Graham, J. P. A. Fairclough, P. D. Olmsted and A. J. Ryan, *Macromolecules*, 2008, **41**, 1901-1904.

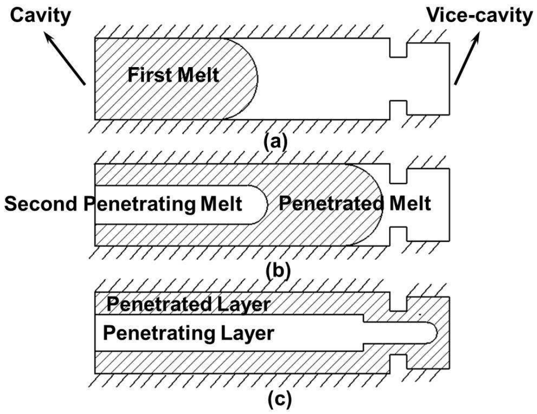

Fig. 1Schematic representation of MFMIM process: (a) partial filling of the first melt; (b) penetration of the second fluid; (c) melt packing stage

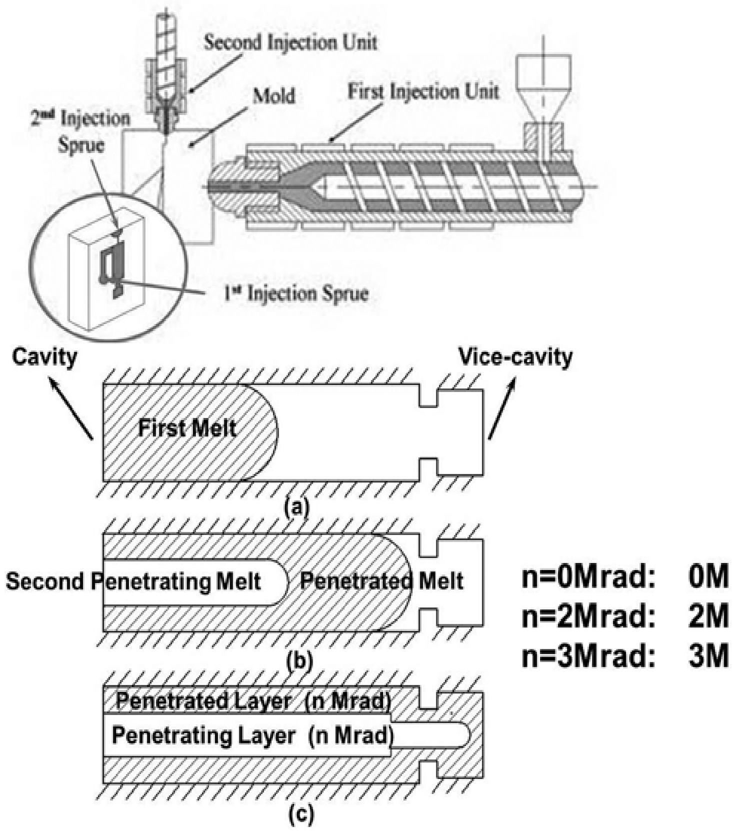

Fig. 2 Schematic representation of the MMMIM instrument utilized.

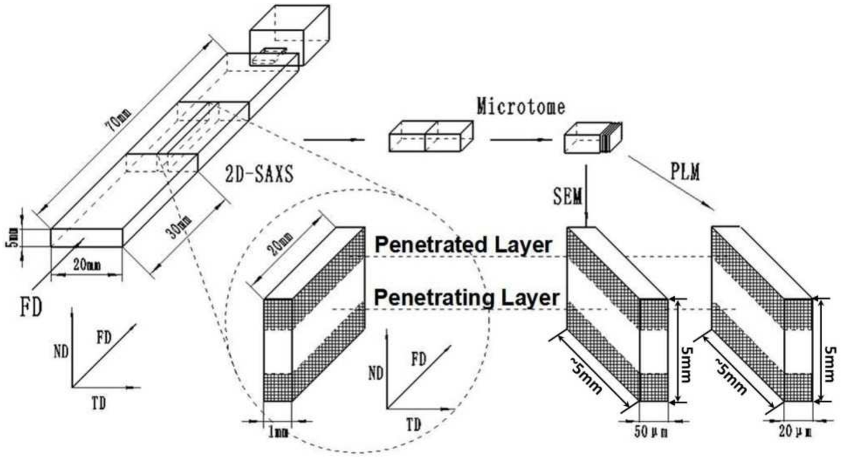

Fig. 3 Schematic representation of sample preparation for SEM, PLM and 2D-SAXS characterizations. FD, the flow direction; TD, the transverse direction; ND, the normal direction to the TD-FD plane.

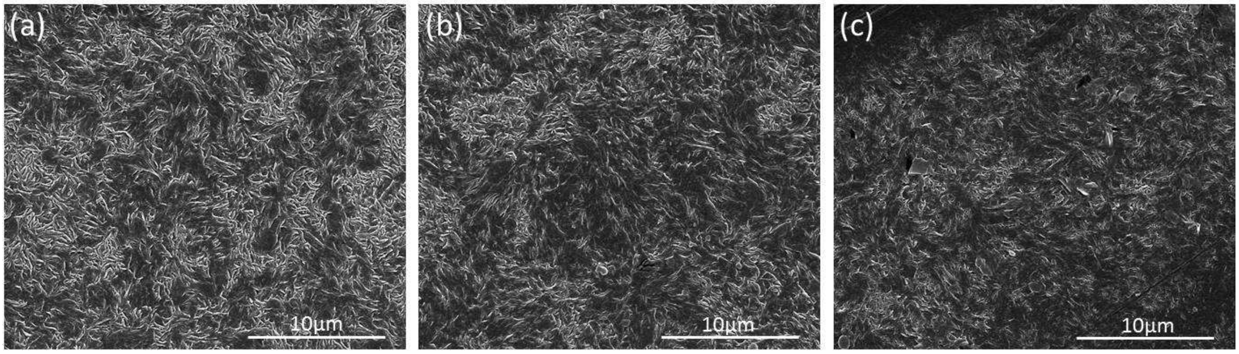

Fig. 4 SEM micrographs in subskin layers of samples with different doses of irradiation molded by CIM: (a) 0C, (b) 2C, (c) 3C.

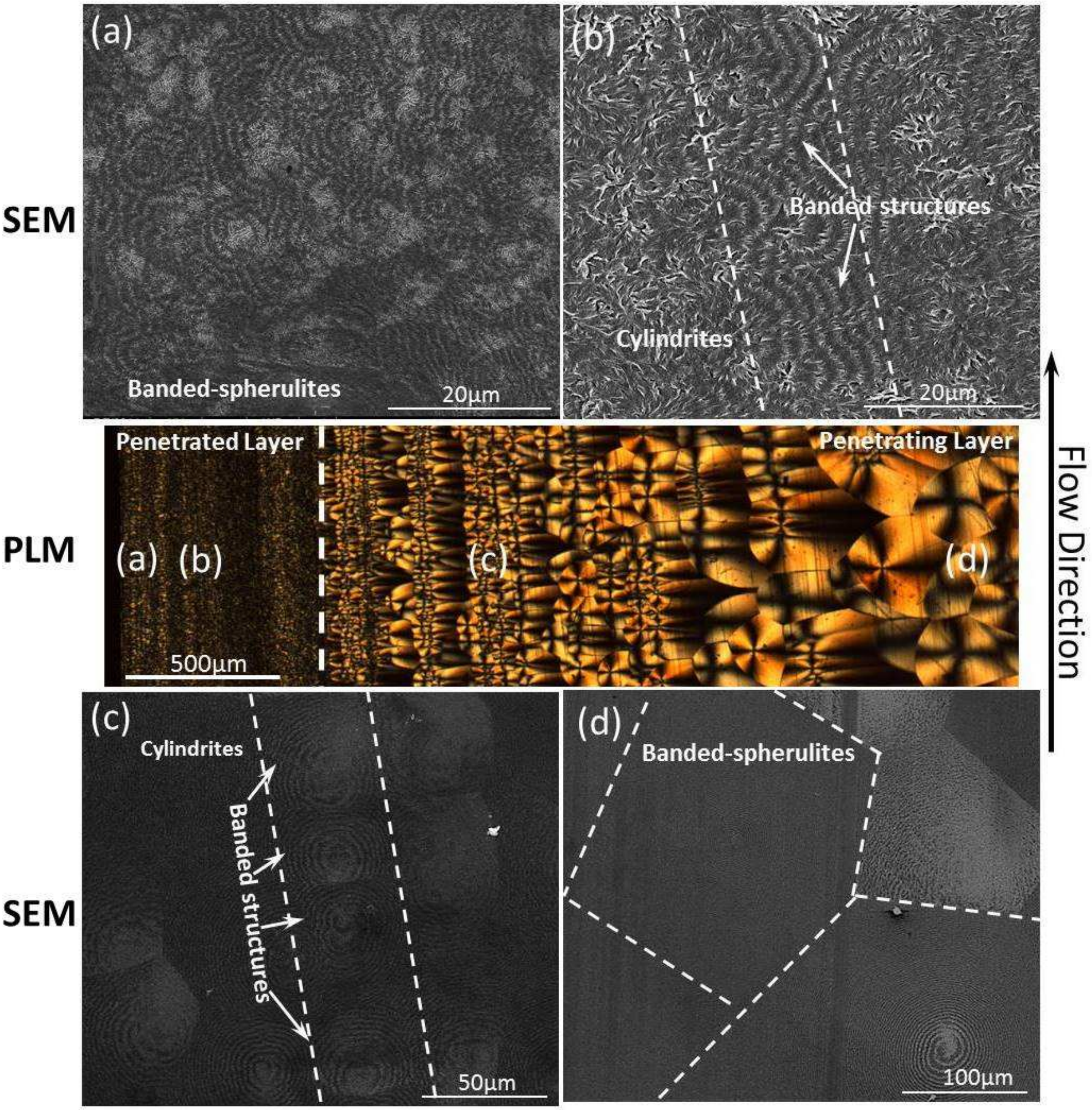

Fig. 5 SEM and PLM micrographs of 0M sample, SEM micrographs are at the top and bottom while the PLM micrograph is in the middle location. Letters a, b, c and d indicating four layers in 0M part were shown in PLM: (a) skin, (b) subskin, (c) transition, (d) core layer.

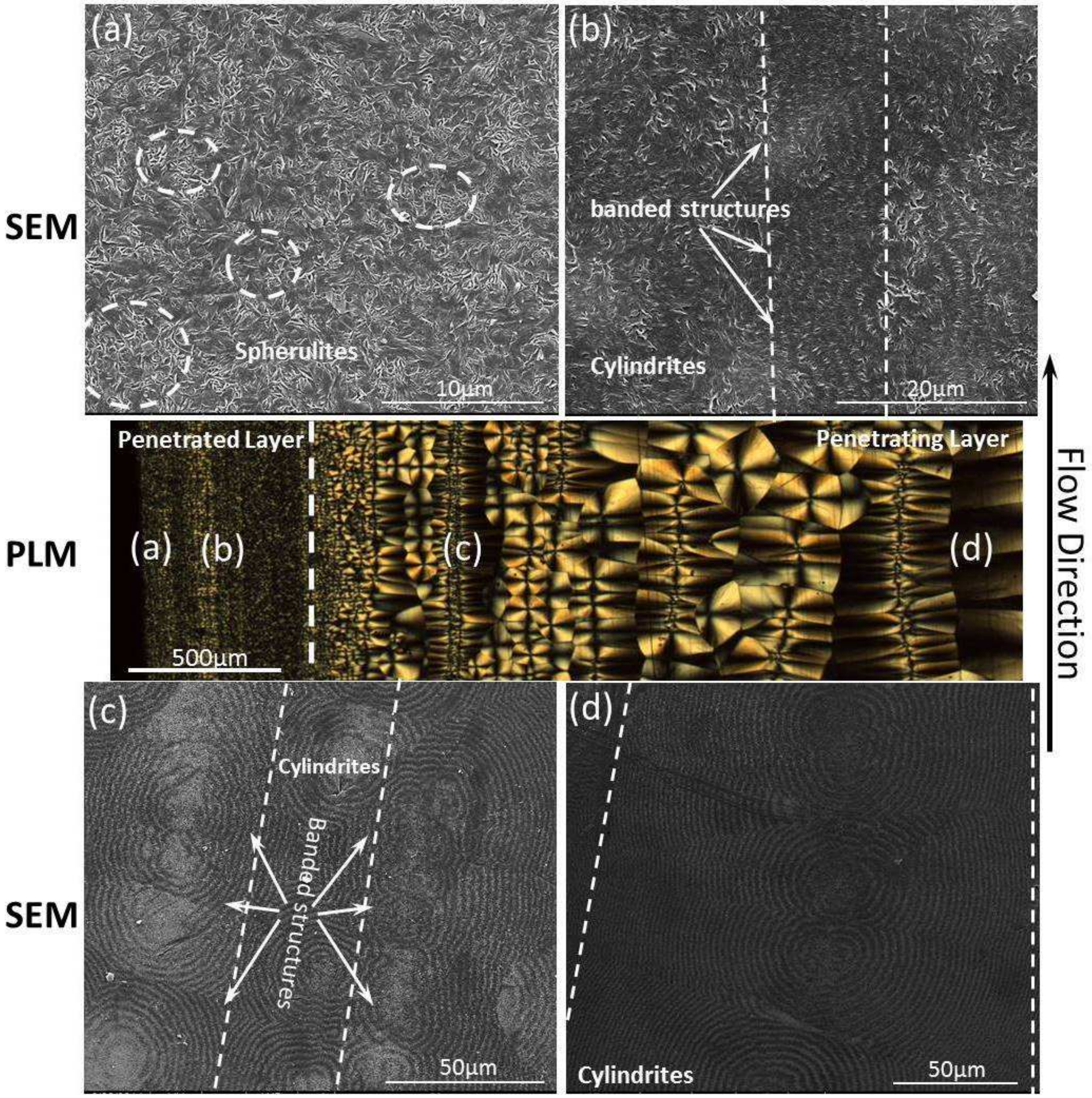

Fig. 6 SEM and PLM micrographs of 2M sample, SEM micrographs are at the top and bottom while the PLM micrograph is in the middle location. Letters a, b, c and d indicating four layers in 2M part were shown in PLM: (a) skin, (b) subskin, (c) transition, (d) core layer.

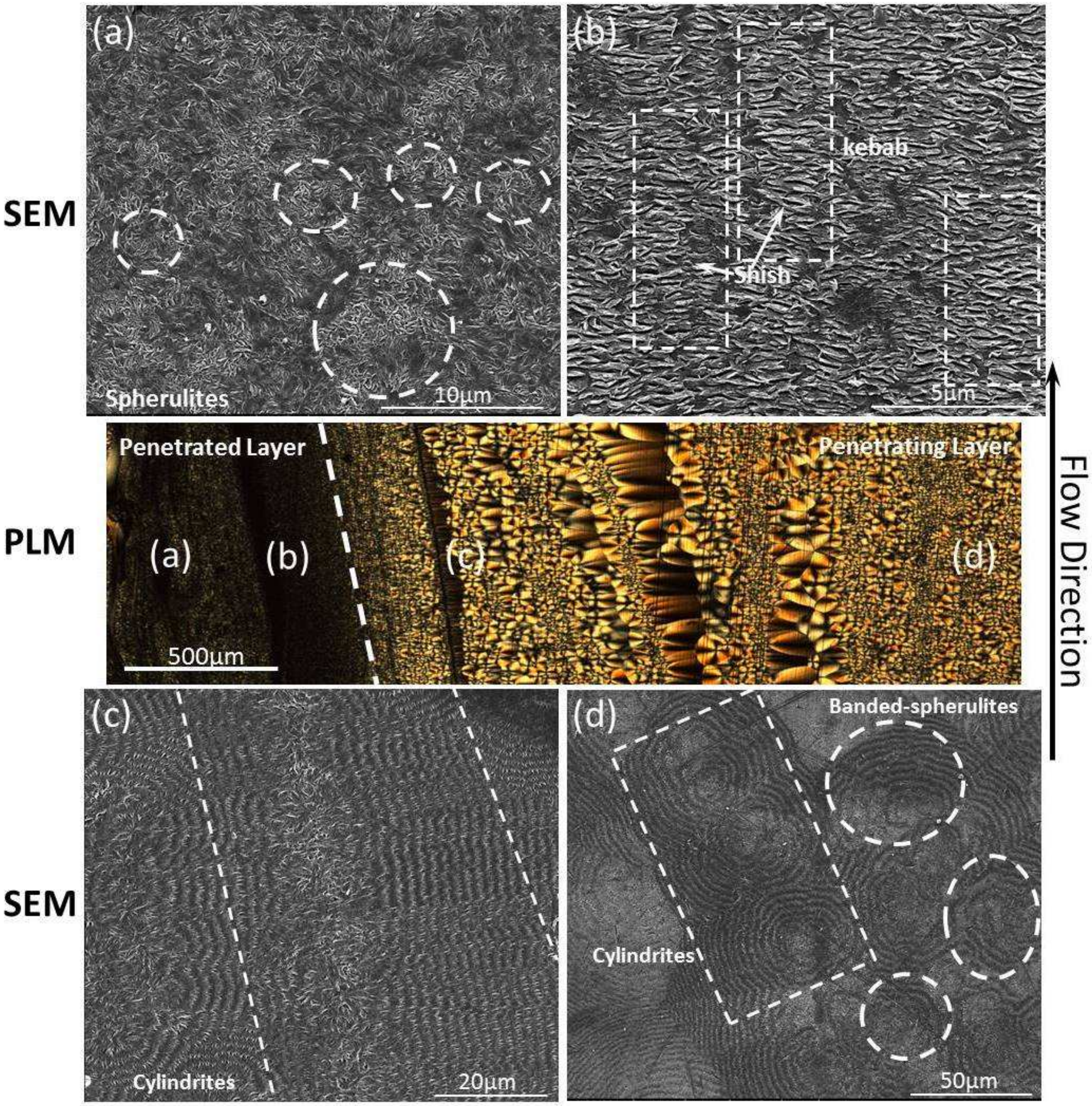

Fig. 7 SEM and PLM micrographs of 3M sample, SEM micrographs are at the top and bottom while the PLM micrograph is in the middle location. Letters a, b, c and d indicating four layers in 3M part were shown in PLM: (a) skin, (b) subskin, (c) transition, (d) core layer.

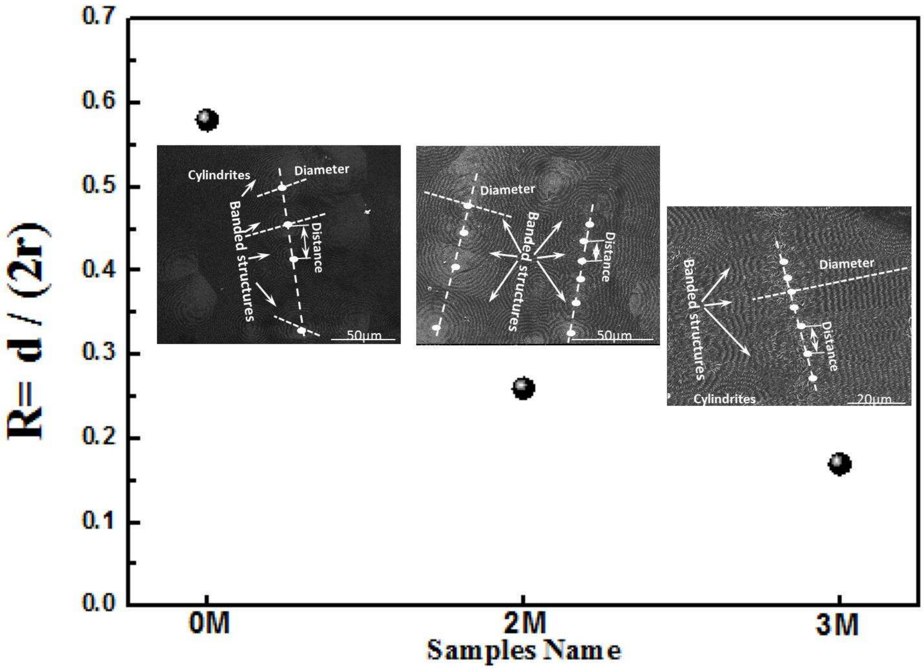

Fig. 8 The averaged ratio (R) of nuclei distance (d) to crystals diameter (2r) in transition layer of three kinds of samples.

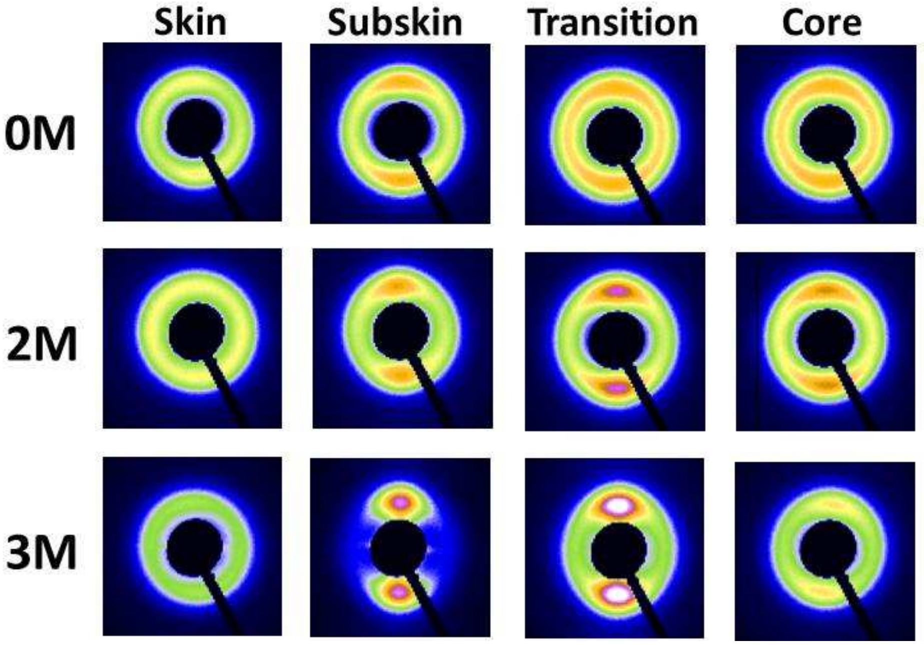

Fig. 9 2D-SAXS patterns at various locations of the samples treated with different doses of irradiation.

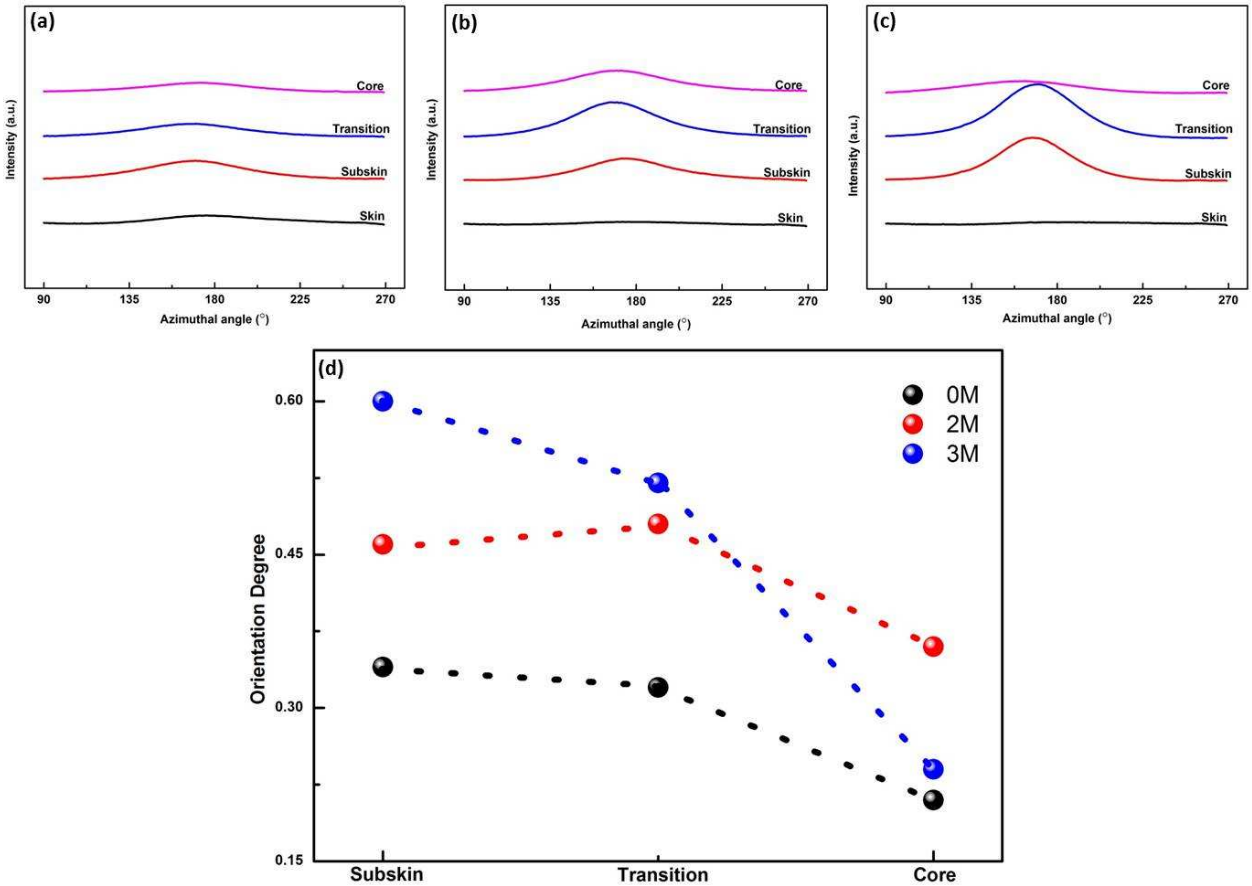

Fig. 10 Scattering intensity distribution along azimuthal angle of samples: (a) 0M, (b) 2M, (c) 3M, (d) the orientation factors in various locations of melt penetration samples.

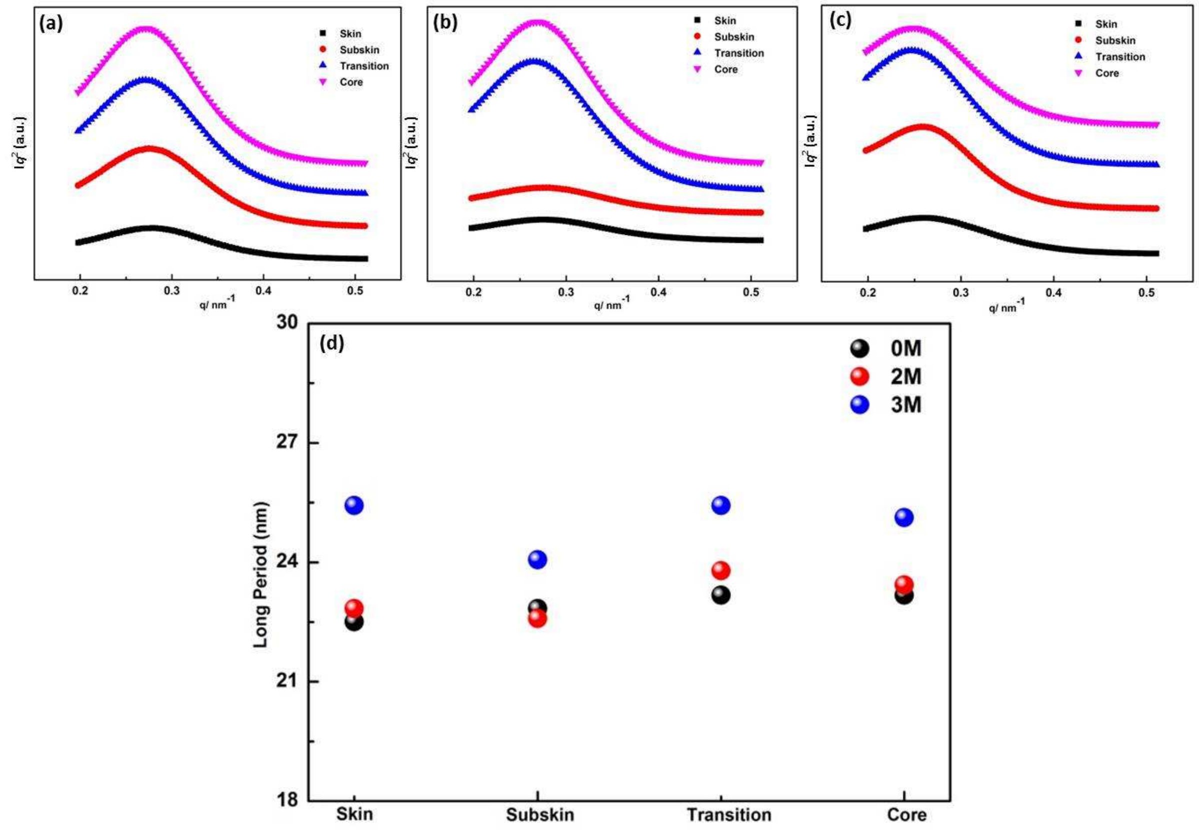

Fig. 11 1D-SAXS intensity profiles along the meridian in various locations of samples: (a) 0M, (b) 2M, (c) 3M, (d) the long period in various locations of melt penetration samples.

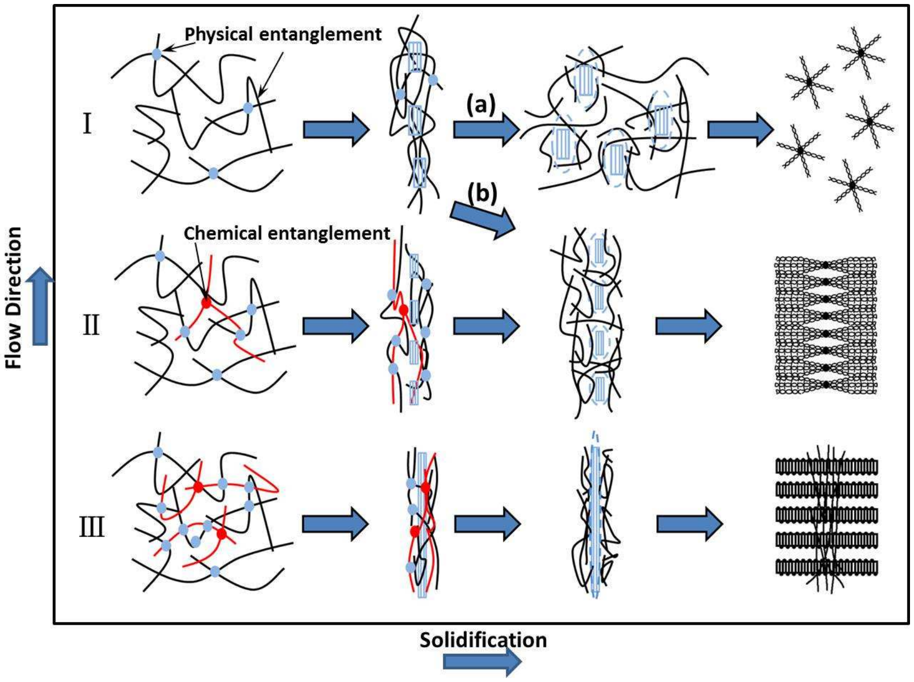

Fig. 12 Schematic representation of the evolution of physical entangled network and permanent entanglements in cross-linked structure under flow.